17. Y. Sakurai *et al.*, *Phys. Rev. Lett.* **74**, 2252 (1995).
18. S. B. Dugdale *et al.*, *Phys. Rev. Lett.* **96**, 046406 (2006).
19. N. Hiraoka, T. Buslaps, V. Honkimäki, J. Ahmad, H. Uwe, *Phys. Rev. B* **75**, 121101(R) (2007).
20. C. Utfeld *et al.*, *Phys. Rev. B* **81**, 064509 (2010).
21. Materials and methods are available as supporting material on *Science* Online.
22. B. Barbiellini *et al.*, *Physica C* **229**, 113 (1994).
23. W. Weyrich, P. Pattison, B. G. Williams, *Chem. Phys.* **41**, 271 (1979).
24. R. Harthoorn, P. E. Mijnarends, *J. Phys. F Met. Phys.* **8**, 1147 (1978).
25. P. E. Mijnarends, *Physica* **63**, 235 (1973).
26. H. Sakakibara, H. Usui, K. Kuroki, R. Arita, H. Aoki, *Phys. Rev. Lett.* **105**, 057003 (2010).
27. A. Bansil, R. S. Rao, P. E. Mijnarends, L. Schwartz, *Phys. Rev. B* **23**, 3608 (1981).
28. A. Bansil, *Z. Naturforsch. A* **48**, 165 (1993).
29. J. B. Goodenough, J. Zhou, *Phys. Rev. B* **42**, 4276 (1990).

Acknowledgments: The work at JASRI was supported by a Grant-in-Aid for Scientific Research (no. 18340111) from the Ministry of Education, Culture, Sports, Science, and Technology (MEXT), Japan, and that at Tohoku University was supported by a Grant-in-Aid for Scientific Research (nos. 16104005, 19340090, and 22244039) from the MEXT, Japan. The work at Northeastern University (NU) was supported by the Division of Materials Science and Engineering, Office of Science, U.S. Department of Energy, and it benefited from the allocation of supercomputer time at the National Energy Research Scientific Computing Center, the NU's Advanced Scientific Computation Center (ASCC), and the Stichting Nationale Computerfaciliteiten (National Computing Facilities Foundation, NCF). The Compton scattering experiments were performed with the approval of JASRI (proposals 2003B0762, 2004A0152, 2007B1413, 2008A1191, and 2010A1907).

Supporting Online Material
www.sciencemag.org/cgi/content/full/science.1199391/DC1
Materials and Methods
Fig. S1

21 October 2010; accepted 22 March 2011
Published online 28 April 2011;
10.1126/science.1199391

Photodetection with Active Optical Antennas

Mark W. Knight,[1,2] Heidar Sobhani,[1,2] Peter Nordlander,[1,2,3] Naomi J. Halas[1,2,3]*

Nanoantennas are key optical components for light harvesting; photodiodes convert light into a current of electrons for photodetection. We show that these two distinct, independent functions can be combined into the same structure. Photons coupled into a metallic nanoantenna excite resonant plasmons, which decay into energetic, "hot" electrons injected over a potential barrier at the nanoantenna-semiconductor interface, resulting in a photocurrent. This dual-function structure is a highly compact, wavelength-resonant, and polarization-specific light detector, with a spectral response extending to energies well below the semiconductor band edge.

Optical antennas are key elements in the conversion of light from free space to ultrasmall, nanometer-scale volumes. The intense light-focusing properties of these structures are due to surface plasmons, oscillations of free electrons in metals that couple to the incident light field. A wide range of applications—in sensing, subwavelength and nonlinear optics, and even novel medical therapies—have arisen for nanoantennas, exploiting the large local electromagnetic fields and intense heating they provide (*1*–*3*). Recent studies have investigated the use of plasmonic antennas to enhance the performance of photoactive devices, such as solar cells, light-emitting diodes, and photodetectors (*4*–*8*). Typically, one or more antennas are placed on or close to the active region of a device, where the near field of the plasmon, the scattering cross section, and the tailored photon density of states may all act to modify and enhance device characteristics.

Another important property of optical antennas is their propensity for generating energetic or "hot" electron-hole pairs by plasmon decay (*9*–*16*). Light not redirected by the antenna is absorbed, forming an energetic electron-hole pair. This process is an additional contribution to plasmon damping, broadening the intrinsic linewidth, and is typically considered deleterious to antenna performance. This process of hot electron generation has been shown to participate in photochemical reactions at noble metal nanoparticle surfaces (*17*–*21*), but it has remained largely unexploited in solid-state devices.

We report an active optical antenna device that uses the hot electron-hole pairs arising from plasmon decay to directly generate a photocurrent, resulting in the detection of light (Fig. 1). This is accomplished by a nanoantenna fabricated on a semiconductor surface where a metal-semiconductor, or Schottky, barrier is formed at the antenna-semiconductor interface. When this type of antenna is photoexcited it generates electron-hole pairs (*9*–*12*) and injects hot electrons into the semiconductor over the Schottky barrier, contributing to a detectable photocurrent (Fig. 1A). In this configuration, photocurrent generation is no longer limited to photon energies above the band gap of the semiconductor, but rather to photon energies above the Schottky barrier height (*22*). Therefore, this device is capable of detecting light well below the band gap of the semiconductor at room temperature and without a bias voltage.

Our initial realization of active optical antenna-diode photodetection consists of an array of independent, rectangular gold nanorods (Fig. 1B) (*23*). Nanorods support both longitudinal and transverse plasmon resonances, with the frequency of these resonances determined by the nanorod geometry: Increasing the nanorod aspect ratio tunes the longitudinal resonance to respond at longer wavelengths (*24*). The resonators studied here had heights and widths of 30 and 50 nm, respectively, and lengths ranging from 110 to 158 nm. Each device array consisted of 300 devices arranged in a 15 × 20 array with a 250-nm interantenna spacing in both the longitudinal and transverse directions, sufficient to ensure that near-field interantenna coupling is absent. The

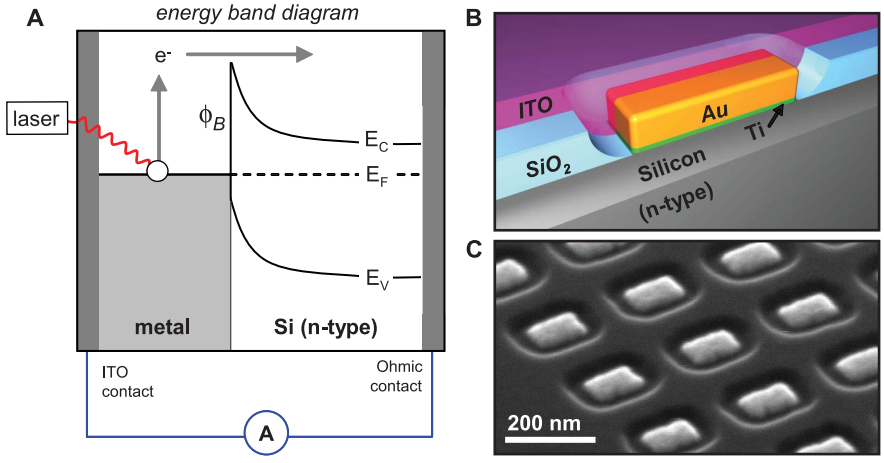

Fig. 1. An optical antenna-diode for photodetection. (**A**) Band diagram for plasmonically driven internal photoemission over a nanoantenna-semiconductor Schottky barrier (ϕ_B). (**B**) Representation of a single Au resonant antenna on an n-type silicon substrate. (**C**) Scanning electron micrograph of a representative device array prior to ITO coating, imaged at a 65° tilt angle.

[1]Department of Electrical and Computer Engineering, Rice University, Houston, TX 77005, USA. [2]Laboratory for Nanophotonics, Rice University, Houston, TX 77005, USA. [3]Department of Physics and Astronomy, Rice University, Houston, TX 77005, USA.

*To whom correspondence should be addressed. E-mail: halas@rice.edu

structure is surrounded by an insulating SiO_2 region (Fig. 1C) and then electrically connected through a top transparent electrode of indium tin oxide (ITO).

The photocurrent obtained from these devices is determined directly by the antenna properties. The photocurrent shows a strong wavelength dependence resulting from the rod geometry, with maximum currents increasing in wavelength with increasing antenna length (Fig. 2A). The spectral response directly follows the longitudinal dipole absorption resonance of the plasmon mode excited on the structure. The polarization dependence of the photocurrent also follows that of the nanoantennas, with a highly polarization-dependent response (Fig. 2B, green points) obeying a $\cos^2\theta$ angular dependence characteristic of a dipole antenna (gray line). For light polarized along the short (transverse) rod axis, we observe >90% attenuation of the photocurrent with respect to the longitudinal polarization. Incident power variation at a single wavelength results in a linear response of the photocurrent, which suggests that the photocurrent is dominated by the conversion of single photons to single hot electrons over this range of incident light intensities (Fig. 2C) (*9*–*12*, *14*).

The responsivity of this device can be understood by first considering a Schottky diode in the absence of a plasmon resonance, where the responsivity depends only on the energy-dependent internal photoemission probability. This quantum transmission probability η_i can be approximated by the modified Fowler theory (*25*, *26*), which describes the number of "available" electrons in the system with sufficient energy to overcome the potential barrier:

$$\eta_i \approx C_F \frac{(h\nu - q\phi_B)^2}{h\nu} \quad (1)$$

where C_F is the device-specific Fowler emission coefficient (*26*), $h\nu$ is the photon energy, and $q\phi_B$ is the Schottky barrier energy. Fitting the responsivity curve of a planar Schottky device with this equation allows one to extract the material-dependent Schottky barrier height for a given metal-semiconductor interface.

When the Schottky barrier is formed by a plasmon resonant antenna rather than a continuous film, the device responsivity R will show a Fowler response modified by the plasmon absorption spectrum S:

$$R(\nu) = \eta_i S(\nu) \quad (2)$$

With this extended Fowler relation, we can extract the Schottky barrier height for devices with a known plasmon line shape. In general, $S(\nu)$ will depend on multiple factors, including the geometry, composition, and size of the plasmonic devices. In the quasi-static regime, where the plasmonic particles are significantly smaller than the wavelength of light, the optical response will be dipolar and will exhibit a Lorentzian line shape near the resonance frequency (*13*). Fitting the experimental responsivities (Fig. 2A) with Eq. 2, using a Lorentzian line shape for $S(\nu)$, yields a Schottky barrier height of 0.50 eV. From this analysis we find that the barrier height is determined primarily by the 1-nm Ti adhesion layer and is consistent with Ti/Si Schottky barrier devices (*27*). This low barrier height should permit a detection window covering the entire short-wave infrared spectral range (λ = 1.2 to 2.5 μm).

Conversely, with a known Schottky barrier height, the absorption spectrum of an antenna diode of arbitrary geometry can be extracted from the spectral dependence of the responsivity. For our system, the experimental absorption spectra extracted from the overall responsivity (Fig. 2C) using a barrier height of 0.50 eV are shown in Fig. 2D. These experimental spectra exhibit extremely close agreement with calculated absorption spectra (Fig. 2E); both spectral sequences exhibit similar peak locations for nominally identical geometries, exhibiting a linear redshift with increasing aspect ratio, as is characteristic for nanorods (*24*, *28*). This agreement is notable given that the finite-difference time domain (FDTD) simulations (Fig. 2E) included no adjustable parameters; all calculations were performed with experimental dimensions and literature values for the optical constants of materials (Si, SiO_2, Au, Ti, ITO) (*29*–*31*). This agreement also shows that although the nanoantennas are configured in an array, their response is that of individual, independent nanoantennas and is consistent with the collected photocurrent being generated by hot carriers injected by each discrete nanoscale device.

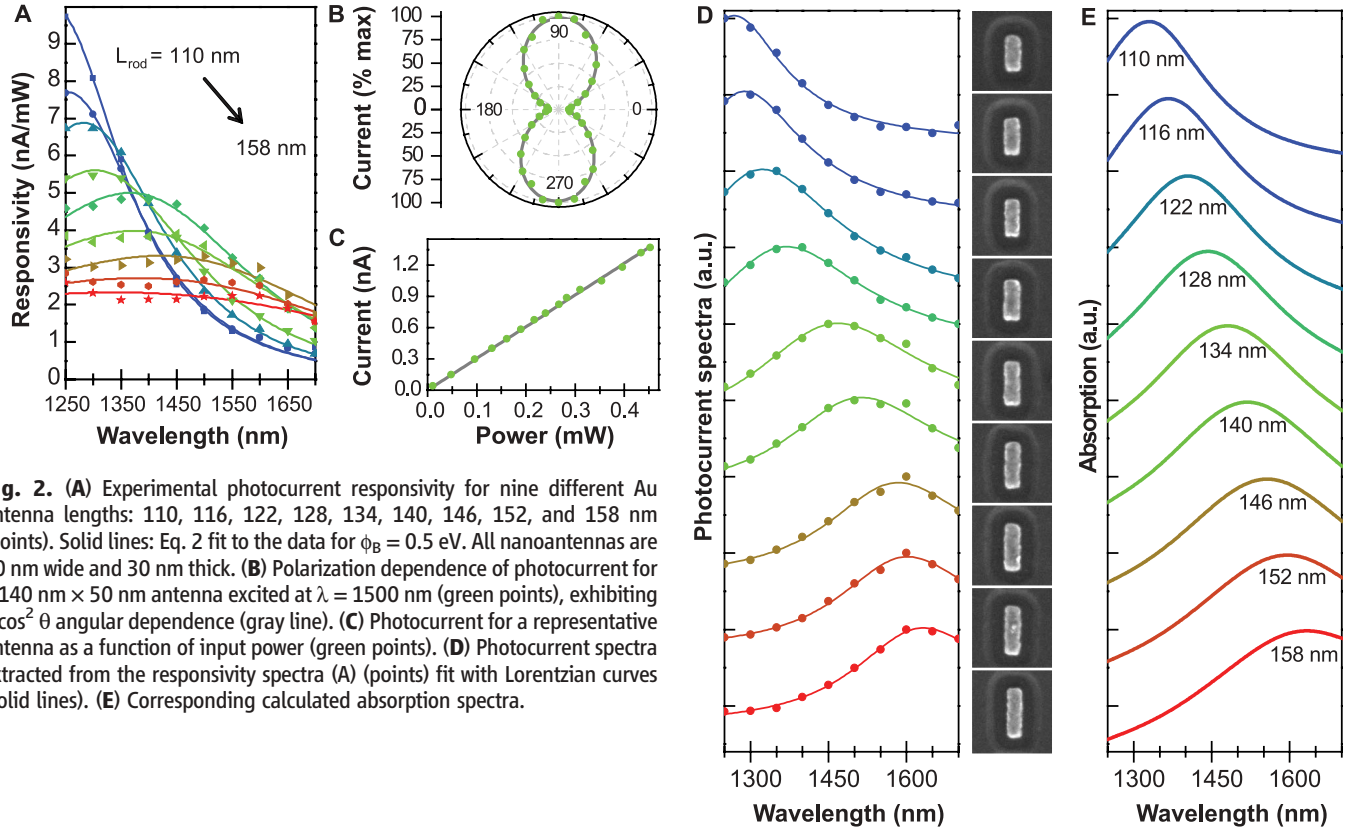

Fig. 2. (**A**) Experimental photocurrent responsivity for nine different Au antenna lengths: 110, 116, 122, 128, 134, 140, 146, 152, and 158 nm (points). Solid lines: Eq. 2 fit to the data for ϕ_B = 0.5 eV. All nanoantennas are 50 nm wide and 30 nm thick. (**B**) Polarization dependence of photocurrent for a 140 nm × 50 nm antenna excited at λ = 1500 nm (green points), exhibiting a $\cos^2\theta$ angular dependence (gray line). (**C**) Photocurrent for a representative antenna as a function of input power (green points). (**D**) Photocurrent spectra extracted from the responsivity spectra (A) (points) fit with Lorentzian curves (solid lines). (**E**) Corresponding calculated absorption spectra.

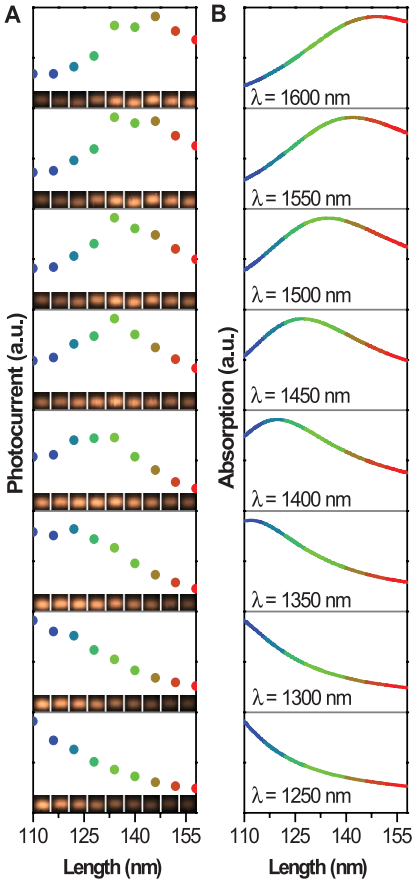

Fig. 3. Sensing the wavelength of incident light. (**A**) Relative photocurrent amplitudes at fixed wavelengths for the nine resonator lengths in Fig. 2. The color coding of the points is the same as in Fig. 2. Insets: Raw photocurrent images (normalized) for each device array. (**B**) Calculated absorption amplitudes for devices that are nominally identical to the experimental system.

When photocurrent measurements are performed on multiple antenna arrays, each with a different resonant frequency, these devices can function as tiny, on-chip spectrometers. This spectroscopic functionality is due to the relationship between photocurrent amplitude and the amplitude of the plasmon resonance at a given frequency. Each antenna array will generate a photocurrent maximum when driven on resonance, with decreasing photocurrent for antennas with a plasmon resonance detuned from the excitation frequency (Fig. 3). The proportionality between photocurrent and relative nanorod resonance amplitudes, expressed in Eq. 2, shows that at a fixed frequency where η_i is nearly constant, the spectral amplitude is directly proportional to device responsivity. Responsivity curves collected using the nine different antenna lengths presented in Fig. 2 are shown in Fig. 3, which illustrates the remarkable agreement between experimental responsivity as a function of antenna resonant frequency and optical absorption amplitudes calculated using the FDTD method. This spectral sensitivity can be used to determine the wavelength of incident light.

The overall quantum efficiency of these nanoantenna-diodes depends on the properties of their constituent materials and the specifics of their device geometry, how these factors affect hot electron generation, and the probability that the hot electrons generated will contribute to the photocurrent. Factors influencing the efficiency of hot electron production include the antenna geometry, the electronic structure of the metal(s) constituting the antenna, and the transmission efficiency of light through the uppermost ITO electrical contact layer. The efficiency of converting hot electrons to photocurrent is affected by the Schottky barrier height, the circuit resistance, and other device-specific parameters. For a device where these factors are known, Eq. 2 permits the direct conversion of experimental photocurrent to absolute absorption cross section.

Although the devices presented here enable us to investigate hot electron generation by plasmonic antennas, further optimization can significantly increase their quantum efficiency (at present, 0.01% of photons absorbed by each nanoantenna are converted into photocurrent). The role of the titanium layer appears to be quite critical: Numerical simulations show that the 1-nm layer is responsible for producing nominally 33% of the hot electrons, which would increase to more than 50% for a 5-nm thickness. Further experimental studies have indicated that reducing extraneous Ti oxidation during the fabrication process, improving ohmic contacts, and increasing the conductivity of the uppermost ITO layer can collectively increase device efficiency by more than an order of magnitude. In addition, a reverse bias of 1 V increases the photocurrent by a factor of 20. Together, these improvements would boost the quantum yield to nearly 2% over the spectral range of the device. A thin dopant layer could also boost efficiency, increase responsivity, and expand the spectral response of the devices by reducing the Schottky barrier height. Applying antireflection coatings or multipass geometries will also further increase the quantum yield.

The range of potential applications of this device concept is extremely diverse. As a silicon-based detector capable of detecting sub–band gap photons, this device could find widespread use in on-chip silicon photonics, ultimately eliminating the need to integrate additional semiconductor materials as detectors into chip designs, which would lower fabrication costs. The photodetection mechanism is compatible with existing, above–band gap photodetectors, which when combined could greatly extend the spectral range of silicon light-harvesting devices, such as silicon-based solar cells, into the infrared region of the spectrum. The broad infrared sensitivity of these devices could enable low-cost silicon infrared imaging detectors that may replace costly InGaAs detectors in this same spectral range. Antenna-diodes also offer functional aspects of photodetection not previously realized. By exploiting nanoantennas as a direct light-harvesting and carrier generation element, both polarization- and wavelength-selective detectors can be realized without additional optical components. We believe this mechanism of photodetection may give rise to additional unforeseen applications in photosensing, energy harvesting, imaging, and light detection technologies.

References and Notes

1. P. Mühlschlegel, H. J. Eisler, O. J. F. Martin, B. Hecht, D. W. Pohl, *Science* **308**, 1607 (2005).
2. S. Lal, S. Link, N. J. Halas, *Nat. Photonics* **1**, 641 (2007).
3. A. M. Gobin *et al.*, *Nano Lett.* **7**, 1929 (2007).
4. H. A. Atwater, A. Polman, *Nat. Mater.* **9**, 205 (2010).
5. T. Ishi, J. Fujikata, K. Makita, T. Baba, K. Ohashi, *Jpn. J. Appl. Phys.* **44**, L364 (2005).
6. N. Yu *et al.*, *Nat. Photonics* **2**, 564 (2008).
7. M. Westphalen, U. Kreibig, J. Rostalski, H. Luth, D. Meissner, *Sol. Energy Mater. Sol. Cells* **61**, 97 (2000).
8. L. Tang *et al.*, *Nat. Photonics* **2**, 226 (2008).
9. J. Hofmann, W. Steinmann, *Phys. Status Solidi* **30**, K53 (1968).
10. J. G. Endriz, W. E. Spicer, *Phys. Rev. Lett.* **24**, 64 (1970).
11. T. Inagaki, K. Kagami, E. T. Arakawa, *Phys. Rev. B* **24**, 3644 (1981).
12. T. Inagaki, K. Kagami, E. T. Arakawa, *Appl. Opt.* **21**, 949 (1982).
13. U. Kreibig, M. Vollmer, *Optical Properties of Metal Clusters* (Springer, New York, 1995).
14. J. Lehmann *et al.*, *Phys. Rev. Lett.* **85**, 2921 (2000).
15. J. T. Stuckless, M. Moskovits, *Phys. Rev. B* **40**, 9997 (1989).
16. V. M. Shalaev, C. Douketis, J. T. Stuckless, M. Moskovits, *Phys. Rev. B* **53**, 11388 (1996).
17. P. L. Redmond, L. E. Brus, *J. Phys. Chem. C* **111**, 14849 (2007).
18. R. Jin *et al.*, *Science* **294**, 1901 (2001).
19. R. Jin *et al.*, *Nature* **425**, 487 (2003).
20. L. Brus, *Acc. Chem. Res.* **41**, 1742 (2008).
21. X. Wu, E. S. Thrall, H. Liu, M. Steigerwald, L. Brus, *J. Phys. Chem. C* **114**, 12896 (2010).
22. C. Scales, P. Berini, *IEEE J. Quantum Electron.* **46**, 633 (2010).
23. See supporting material on *Science* Online.
24. J. Pérez-Juste, I. Pastoriza-Santos, L. M. Liz-Marzan, P. Mulvaney, *Coord. Chem. Rev.* **249**, 1870 (2005).
25. R. H. Fowler, *Phys. Rev.* **38**, 45 (1931).
26. S. M. Sze, K. K. Ng, *Physics of Semiconductor Devices* (Wiley, Hoboken, NJ, ed. 3, 2007).
27. A. M. Cowley, *Solid-State Electron.* **12**, 403 (1970).
28. C. J. Murphy, N. R. Jana, *Adv. Mater.* **14**, 80 (2002).
29. S. Laux *et al.*, *Thin Solid Films* **335**, 1 (1998).
30. E. D. Palik, Ed., *Handbook of Optical Constants of Solids* (Academic Press, San Diego, CA, 1998), vol. 3.
31. P. B. Johnson, R. W. Christy, *Phys. Rev. B* **6**, 4370 (1972).

Acknowledgments: We thank J. B. Lassiter, J. Day, R. Huschka, A. Schlather, and S. Lal for their insight and input. Supported by NSF Integrative Graduate Research and Educational Training program in Nanophotonics grant DGE-0504425 (M.W.K.), National Security Science and Engineering Faculty Fellowship program of the U.S. Department of Defense grant N00244-09-1-0067, Robert A. Welch Foundation grants C-1220 and C-1222, Office of Naval Research grant N00014-10-1-0989, Air Force Office of Scientific Research grant F49620-03-C-0068, and the Center for Advanced Solar Photophysics, an Energy Frontier Research Center funded by the U.S. Department of Energy.

Supporting Online Material

www.sciencemag.org/cgi/content/full/332/6030/702/DC1
Materials and Methods

19 January 2011; accepted 21 March 2011
10.1126/science.1203056